Characteristics of High-Pressure Liquid–Solid Fluidization

Tsao-Jen Lin and Liang-Shih Fan
Dept. of Chemical Engineering, The Ohio State University, Columbus, OH 43210

Fundamental characteristics of liquid–solid fluidization at high pressures (up to 21 MPa) and moderate temperatures (up to 89°C) are investigated. Properties under study include minimum fluidization velocity (u_{mf}), bed voidage at minimum fluidization, and bed expansion. Devices for in-situ measurements of physical properties of the liquid in the bed are developed, and measurements are carried out to quantify the pressure and temperature effects on the fluidization behavior. The results indicate that under high pressures and moderate temperatures, liquid–solid fluidization behavior is affected significantly by the variation of liquid density and viscosity with pressure. As the pressure increases, the liquid viscosity and density increase, yielding an increased drag force and buoyancy force on the particles, and hence a decreasing u_{mf} and an increasing bed expansion for a given liquid flow rate. An increase in temperature has an opposite effect on the physical properties of the liquid, increasing u_{mf} and decreasing the bed expansion for a given liquid flow rate. Various correlations proposed in the literature for u_{mf} and bed expansion, including those by Richardson and Zaki (1954) and Chitester et al. (1984), are applicable to high-pressure and high-temperature conditions when proper account is made of the liquid physical properties under bed operating conditions.

Introduction

Gas–liquid–solid fluidized beds for industrial applications such as hydrogenation reactions are often carried out at high pressures (Fan, 1989). Important parameters in characterizing the hydrodynamics of liquid–solid fluidization are the bed expansion and the minimum fluidization velocity. Knowledge of the variation of these two parameters with operating conditions (e.g., liquid velocity and liquid physical properties, particle properties, and column geometry) is essential to the design and operation of these fluidization systems.

High-pressure liquid–solid fluidization represents a limiting case of three-phase fluidized-bed operations. Hydrodynamics of liquid–solid fluidization under ambient condition have been extensively studied and reviewed (e.g., Rietema, 1982; Kwauk, 1992; Di Felice, 1995). Many empirical correlations were proposed to describe the hydrodynamic behavior of the bed, for example, the Richardson and Zaki (1954) equation for bed expansion and the Wen and Yu (1966) equation for minimum fluidization velocity, u_{mf}. Little is known regarding the pressure and temperature effects on the characteristics of liquid–solid fluidization.

Pressure and temperature affect the hydrodynamics of liquid–solid fluidization by changing liquid properties such as density and viscosity. Studies of these effects for liquid–solid fluidization are limited only to ambient pressure conditions. With measuring pressure at a given temperature, the liquid density and viscosity increase, leading to an increase in the drag force of the particle. At a given pressure, increasing temperature has an opposite effect on the liquid density and viscosity, and hence the drag force of the particle; thus, in quantifying the liquid–solid fluidization hydrodynamics at elevated pressures and temperatures, the liquid properties must be known.

In this article, the experimental data for the minimum fluidization velocity and bed expansion of liquid–solid fluidization at high pressures and moderate temperatures are presented. Techniques are developed to perform *in situ* measurements of the liquid density and viscosity. The values ob-

tained for these liquid properties are used in the hydrodynamic property analysis. Application to high pressure of the well-known equations developed for ambient conditions is discussed.

Experimental

Flow visualization apparatus

The diagram of the experimental system for high-pressure and high-temperature studies is given in Figure 1. The system consists of a vertical column, a liquid supply tank, a liquid exhaust reservoir, a piston pump, and a pulsation damper. The vertical column comprises plenum, test, and disengagement sections. The liquid supply tank is jacketed with electric heaters that provide desirable temperatures. The pipes and column are insulated. The column is made of stainless steel and is 80 cm in height and 5.08 cm in diameter. Three pairs of plane windows made of quartz are installed on the column; each window is 12.4 mm wide and 92 mm long. These windows allow viewing throughout the entire test section of the column. The present experiments are conducted at pressures up to 21 MPa and temperatures up to 89°C. The pressure is controlled by a back pressure regulator installed at the outlet of the bed. A perforated plate with 37 square pitched holes of 2.4 mm diameter is used as the liquid distributor. Uniformly sized spherical glass beads with $d_p = 0.5$, 1.0, and 2.1 mm, and $\rho_p = 2{,}537$, 2,553, and 2,513 kg/m^3, respectively, are used as the solid phase. The liquid velocities required to achieve minimum fluidization are determined from the relationship between the dynamic pressure drop and the superficial liquid velocity. The bed expansion is determined from direct flow visualization. Paratherm NF heat-transfer fluid, a stable organic liquid ($T_b = 327$°C at 0.1 MPa), is used as the liquid phase. The liquid has the following physical properties: $\mu = 0.032$ kg/m·s and $\rho_f = 869$ kg/m^3 at 25°C and 0.1 MPa.

In situ liquid-property measurements

The properties of the liquid at elevated pressures and temperatures are measured in the column. The bed is pressurized by nitrogen gas. The contribution of liquid vapor can be neglected due to its low vapor pressure ($V_p = 2\times10^{-5}$ MPa at 150°C and 0.1 MPa). In order to maintain a constant temperature for the system, the nitrogen gas is preheated by a gas heater to the desired temperature before being introduced into the column.

Density Measurement. The hydrostatic weighing method is adopted to measure the liquid density at elevated pressures and temperatures. A cylindrical aluminum tube 0.305 m in length and 7.14 mm in outside diameter, shown in Figure 2a, has an adjustable metal weight that is submerged in the liquid. The volume of the tube above the liquid surface varies with the liquid density, specifically, the liquid density relates to the tube volume above the liquid surface based on the Archimedes principle:

$$S[\rho_f l_1 + \rho_g (l - l_1)] = (m_1 + m_2) + S_1 \rho_g l_2, \qquad (1)$$

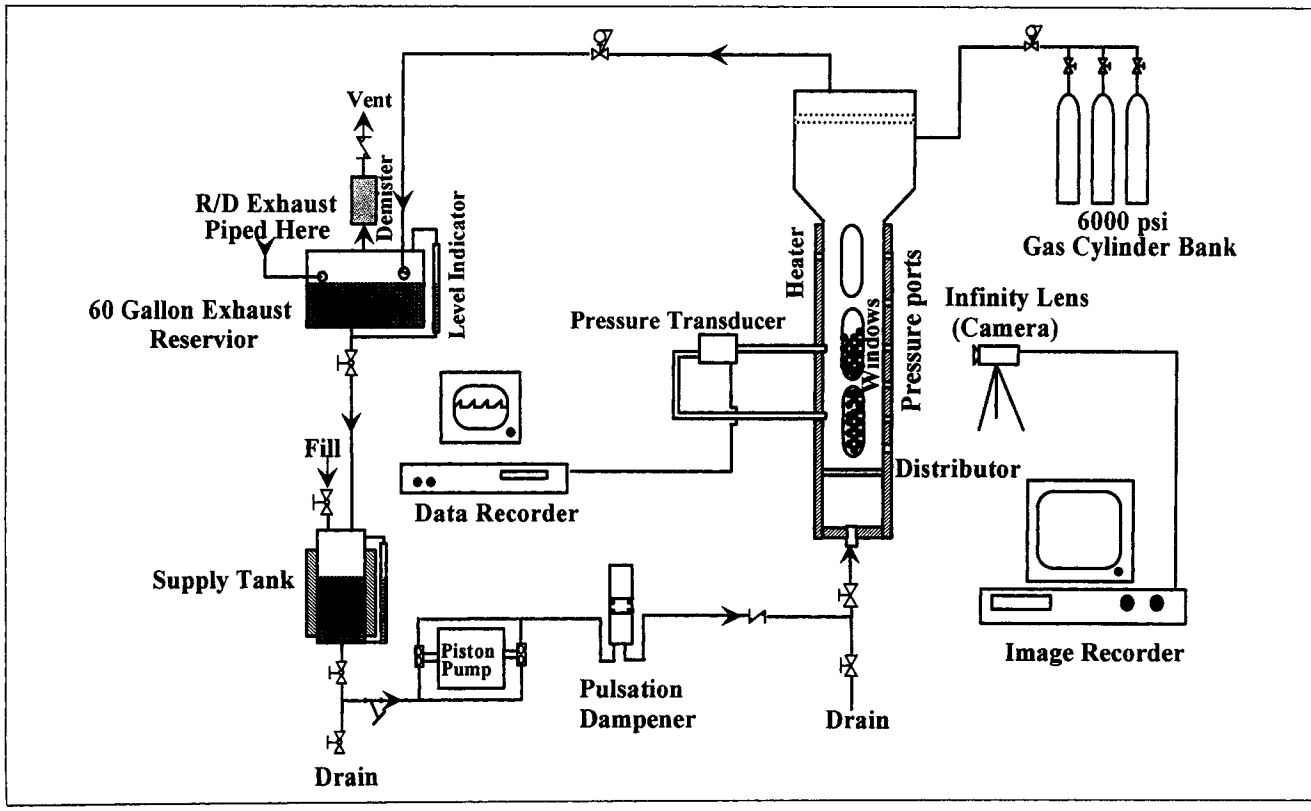

Figure 1. High-pressure and high-temperature liquid solid flow visualization apparatus.

SI conversion: L = gal × 3.79; kPa = psi × 6.89.

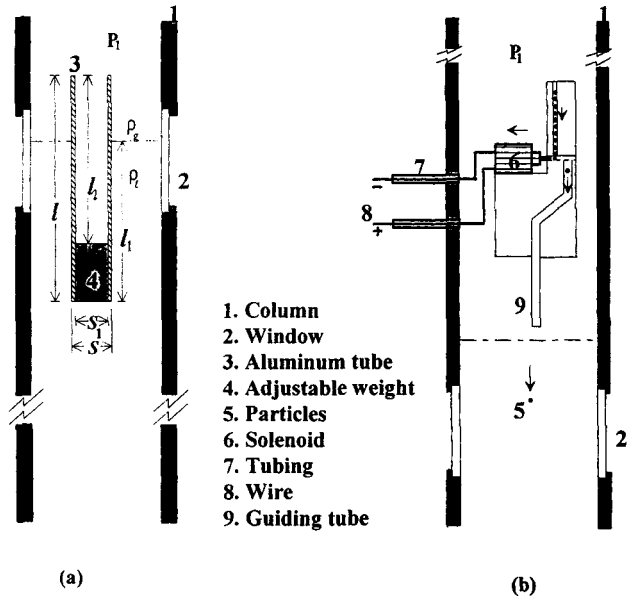

Figure 2. Experimental setup for the measurement of (a) liquid density and (b) viscosity.

where m_1 and m_2 are the masses of the aluminum tube and the adjustable metal weight, respectively; ρ_f and ρ_g are the densities of liquid and pressurized nitrogen gas, respectively; and S and S_1 are the cross-sectional areas of the tube based on the outer and inter diameters, respectively.

Viscosity Measurement. The viscosity of the liquid under elevated pressures and temperatures is determined using the falling-ball technique. The technique is implemented using the system shown in Figure 2b, which consists of a ball-releasing device and a guiding tube. The magnetically operated ball-releasing device is placed inside the column to release the ball into the guiding tube. The falling process is recorded by the CCD camera with an infinity lens situated outside the window. At steady state, the terminal velocity of the falling ball can be calculated from the falling distance (L) and the elapsed time (Δt). For this measurement, nylon particles with sphericity $= 10^{-6}$ m and $\rho_p = 1{,}130$ kg/m^3 are used. The particle size selected is such that the particle Reynolds number, Re_t, is less than 2.

Results and Discussion

In-situ liquid properties

Density. Figure 3a shows the density variation with pressure and temperature for Paratherm NF heat-transfer fluid. In general, liquid compressibility can be negligible for a small variation of pressure; however, for a large variation of pressure, the intermolecular distance significantly decreases, causing the density to increase. From Figure 3a, it can be seen that the density below the normal boiling point increases by about 5% when the pressure increases from ambient pressure to 21 MPa. An increase in temperature results in an increase in the free energy of the fluid, enhancing intermolecular movement and yielding a reduction in the density. Figure 3a shows that the density decreases by about 6% when the temperature increases from 20 to 120°C under the entire pressure range studied.

Viscosity. The molecular structures of the liquid used in this study are complex; there is no theoretical equation that is able to accurately estimate the viscosity of this liquid. Thus, direct measurements using such methods as falling-ball and plate-and-cone or couette-type viscometers are the only alternative. In the direct measurement of liquid viscosity conducted in this study, the falling-ball method is used. The

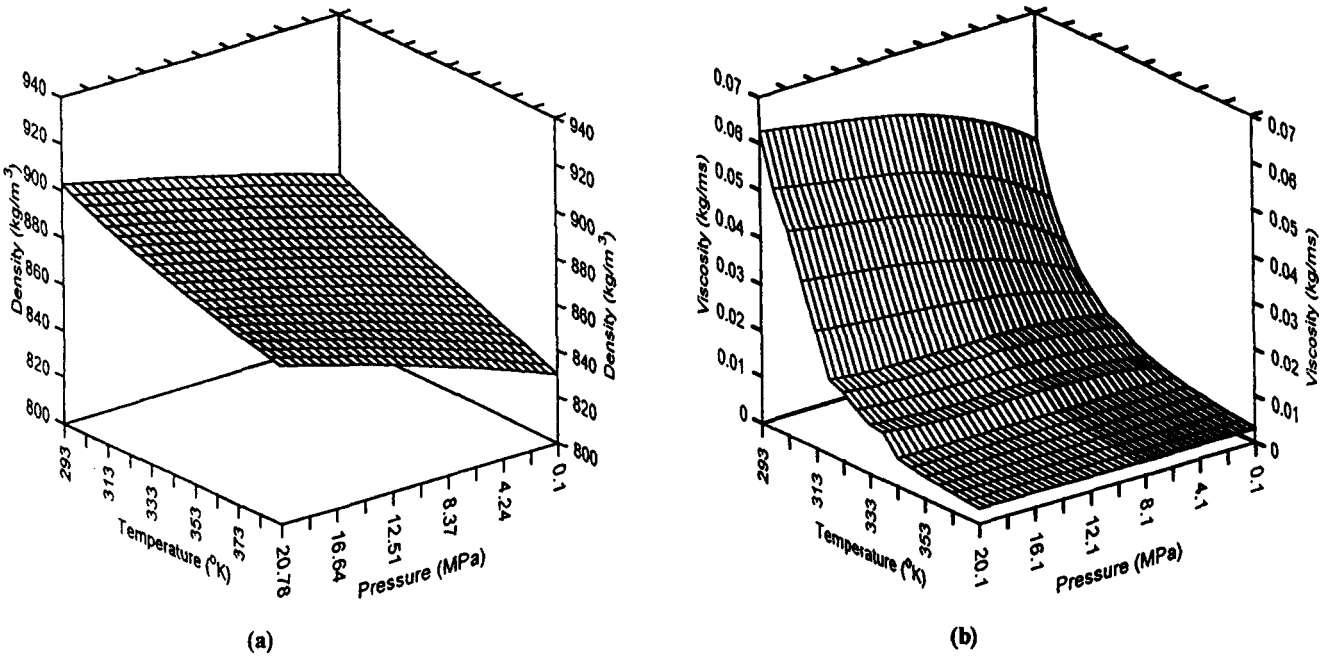

Figure 3. Variations of (a) density and (b) viscosity of Paratherm NF heat-transfer fluid with pressures and temperatures.

Reynolds number based on the particle diameter is maintained in all experiments at less than 2 by varying the particle sizes. The Stokes (1851) and Oseen (1910) equations given below are applied to calculate the viscosity for different flow regimes, based on the Reynolds number:

$$\mu = f_w \frac{d_p^2(\rho_p - \rho_f)g\Delta t}{18L} \qquad (Re_t < 0.1) \qquad (2)$$

$$\mu = f_w \frac{d_p^2(\rho_p - \rho_f)g\Delta t}{18L(1+3Re_t/16)} \qquad (0.1 < Re_t < 2), \qquad (3)$$

where f_w is the correction factor accounting for the wall effect, and can be expressed by (Khan and Richardson, 1987)

$$f_w = 1 - 1.15(d_p/D)^{0.6}. \qquad (4)$$

Figure 3b shows the variations of the viscosity with pressure and temperature for Paratherm NF heat-transfer fluid. The results are partially verified by comparing the measurements with values provided by the Paratherm supplier at a pressure of 0.1 MPa and temperatures below the boiling point. The differences between the measured values and the supplier's results are less than 1%.

In general, the liquid molecules move within parallel liquid layers, where they change their sites by surpassing the activation energy barrier (Ewell and Eyring, 1937). As the pressure increases at low temperatures, the liquid exerts a larger frictional drag on adjacent layers, and the velocity gradient decreases, which causes the viscosity to increase significantly. For high temperatures, however, the liquid molecules have excess free energy to overcome the energy barrier, and thus an increase in pressure does not significantly affect the liquid viscosity. Figure 3b shows that when the pressure increases from 0.1 to 21 MPa, the viscosity for Paratherm NF heat-transfer fluid increases by 65% at 20°C, but only by 10% at 100°C. Figure 3b also indicates that the effect of temperature on the liquid viscosity is more significant than that of pressure.

Macroscopic phenomena

In liquid–solid fluidization, the fluidized particles are balanced by the effective gravitational force F_{eg} (which includes the gravitational force and the buoyancy force) and the drag force F_D induced by the liquid flow as given by

$$F_{eg} = \frac{1}{6}\pi d_p^3(\rho_p - \rho_f)g = F_D. \qquad (5)$$

Define the voidage function $f(\epsilon)$ as (Wen and Yu, 1966)

$$f(\epsilon) = \frac{F_D}{F_{DS}}, \qquad (6)$$

where F_D is the drag force of a single particle in a liquid–solid fluidized bed, and F_{DS} is the drag force of a single particle in the infinite fluid, which can be expressed as $C_D(\rho_f u^2/2)(\pi d_p^2/4)$. $f(\epsilon)$ has been proposed to have the form of ϵ^β (Wen and Yu, 1966; Richardson and Jeronimo, 1979; Foscolo et al., 1983). For the range of $Re < 500$, the coefficient β has a constant value of -4.7. Combining Eqs. 5 and 6 gives

$$\epsilon^{-4.7} = \frac{F_{eg}}{F_{DS}} = \frac{\frac{1}{6}\pi d_p^3(\rho_p - \rho_f)g}{C_D\left(\frac{1}{2}\rho_f u^2\right)\left(\frac{\pi}{4}d_p^2\right)}, \qquad (7)$$

where C_D is the drag coefficient for a single particle in the infinite fluid, which can be correlated for various flow regimes (Khan and Richardson, 1987). The correlation for C_D was given by Clift et al. (1978) for $Re \le 22$ as

$$C_D = \frac{24}{Re}[1 + 0.1315Re^{(0.82 - 0.05\log Re)}]. \qquad (8)$$

Equations 7 and 8 lead to

$$\frac{1}{6}\pi d_p^3(\rho_p - \rho_f)g = \epsilon^{-4.7}\left[\pi\rho_f u^2 d_p^2\left(\frac{3}{Re} + 0.3945\,Re^{-0.18 - 0.05\log Re}\right)\right]. \qquad (9)$$

Figure 4 compares the voidage between the calculated results based on Eq. 9 and the experimental data obtained in this study. It is seen that the calculated results match the experimental data well; some deviations are noted at higher voidage due to the limitation in applicability of the C_D equation. By using the *in-situ* physical properties of the liquid, therefore, Eq. 7 can be applied to account for the voidage variation in liquid–solid fluidization under various operating conditions.

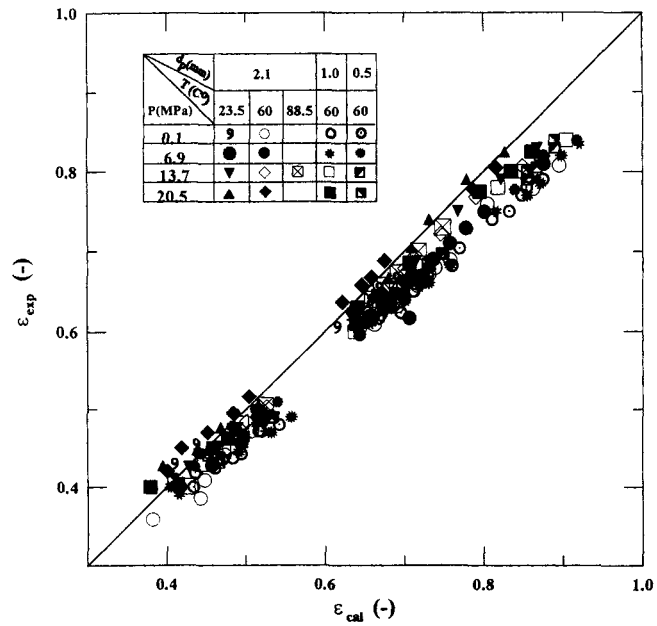

Figure 4. Comparisons of the bed voidage calculated from Eq. 9 with experimental data.

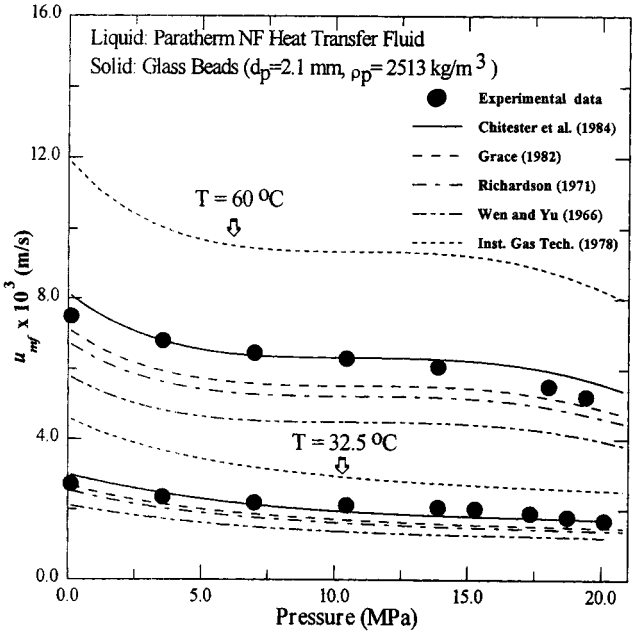

Figure 5. Pressure effects on the minimum fluidization velocity at T = 32.5 and 60°C.

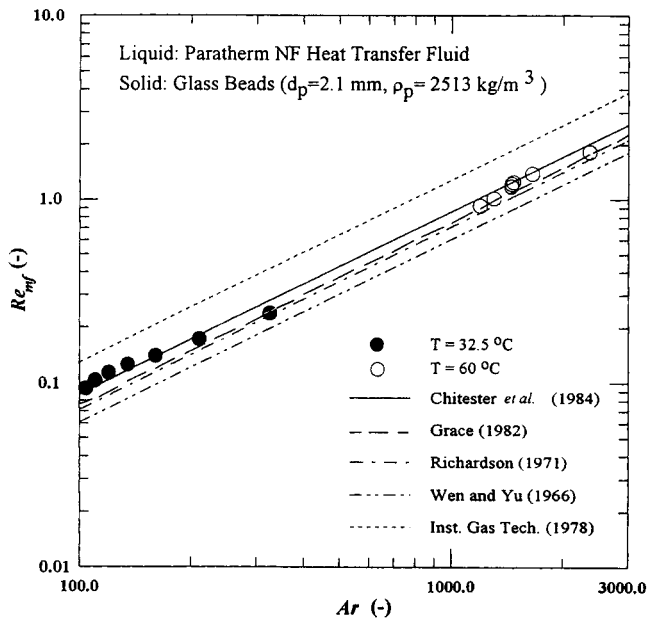

Figure 6. Relationship between Re_{mf} and Ar for minimum fluidization at T = 32.5 and 60°C.

Minimum fluidization

The minimum fluidization velocity, u_{mf}, for various pressures (up to 20 MPa) is studied at T = 32.5 and 60°C, using 2.1-mm glass beads. Figure 5 shows the pressure effect on u_{mf}. The figure indicates that u_{mf} decreases with increasing pressures at a given temperature. From the discussion on the liquid properties given earlier, it is noted that when the pressure increases from 0.1 to 20 MPa both the density and viscosity of the liquid increase significantly, with the rate of increase for the liquid density lower than that for the liquid viscosity. The increase in the density and viscosity of the liquid gives rise to a decreased u_{mf}.

In Figure 5, the pressure effect on u_{mf} at low temperatures is greater than that at high temperatures. For example, when the pressure increases from 0.1 to 20 MPa, u_{mf} decreases by 40% at 32.5°C, but only by 30% at 60°C. This is because the pressure effect on the liquid viscosity at 32.5°C is greater than that at 60°C; hence, at low temperatures the magnitude at which the drag force increases is greater, resulting in a higher decreasing rate of u_{mf}. The pressure and temperature effects can be presented in a plot of Re_{mf} vs. Ar, as shown in Figure 6. It is seen that all data obtained for minimum fluidization are in the laminar flow regime ($Re_{mf} \leq 10$). The general form of the empirical equations for u_{mf} reported in the literature (e.g., Wen and Yu, 1966; Richardson, 1971; Institute of Gas Technology, 1978; Grace, 1982; Chitester et al., 1984) as given below is examined:

$$u_{mf} = \frac{\mu}{\rho_f d_p}\left(\sqrt{C_1^2 + C_2 Ar} - C_1\right), \tag{10}$$

where the constants C_1 and C_2 are described in Table 1. Calculation of u_{mf} based on these equations is presented in Figures 5 and 6, where the liquid physical properties used in calculating u_{mf} are taken from measurements obtained in this study (Figure 3). In Figures 5 and 6 all correlations seem to predict the correct trend, and Chitester et al.'s (1984) equation provides the best fit to the experimental data, while the Institute of Gas Technology (1978) overpredicts and the others underpredict the experimental results.

The effects of pressure on the minimum fluidization voidage ϵ_{mf}, are shown in Figure 7. The figure indicates that as the pressure increases, ϵ_{mf} increases initially, and then decreases after reaching a maximum value. The maximum value of ϵ_{mf} is also observed to be a function of temperature. This behavior can be attributed to the pressure and temperature effects on the liquid properties, which in turn affect the drag force and the buoyancy force. The relationship among temperature, pressure, and ϵ_{mf} can be accounted for by the force balance. It is noted from Figure 6 that the flow under the minimum fluidization condition is in the laminar flow regime. Under minimum fluidization conditions, Eq. 9 gives rise to

$$\frac{\pi}{6} d_p^3 (\rho_p - \rho_f) g = \epsilon_{mf}^{-4.7}\left[\pi \rho_f u_{mf}^2 d_p^2 \left(\frac{3}{Re_{mf}} + 0.3945\, Re_{mf}^{-0.18 - 0.05 \log Re_{mf}}\right)\right]. \tag{11}$$

The values of F_{eg} and F_{DS} at minimum fluidization vary with pressure and temperature. Figure 8 shows the effect of pres-

Table 1. Values of Two Constants in Eq. 10

Reference	C_1	C_2
Wen and Yu (1966)	33.7	0.0408
Richardson (1971)	25.7	0.0365
Institute of Gas Technology (1978)	25.25	0.0651
Grace (1982)	27.2	0.0408
Chitester et al. (1984)	28.7	0.0494

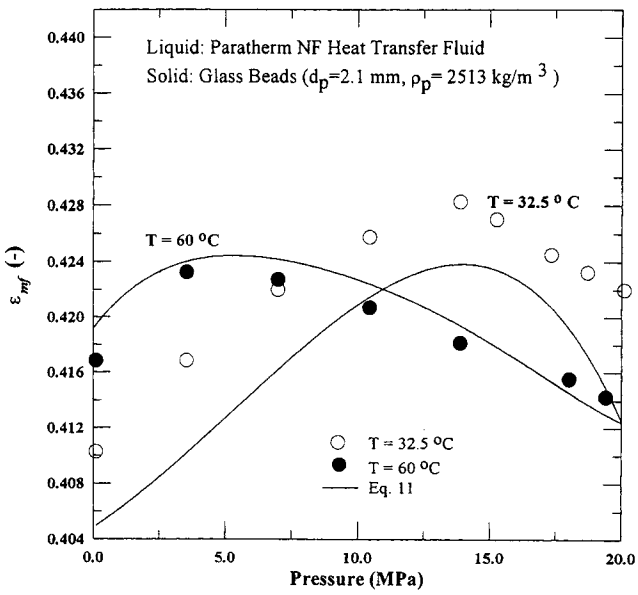

Figure 7. Pressure effects on the minimum fluidization voidage at $T = 32.5$ and 60°C.

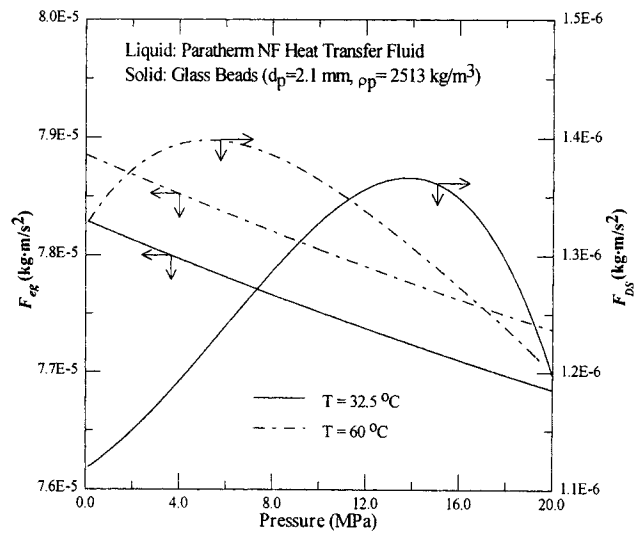

Figure 8. Pressure effects on F_{eg} and F_{DS} at $T = 32.5$ and 60°C under minimum fluidization conditions.

sure on F_{eg} and F_{DS} under minimum fluidization for $T = 32.5$ and 60°C. The figure indicates that at a given temperature, F_{eg} decreases with pressure because the liquid density increases with pressure. With an increase in pressure, F_{DS} initially increases due to the change in the liquid density and viscosity; the decrease in u_{mf} then becomes dominant, which leads to a decrease in F_{DS}. The bed voidage at minimum fluidization, ϵ_{mf}, can be calculated from Eq. 11, as shown in Figure 7. The figure shows that the calculated values for ϵ_{mf} match the data reasonably well.

Bed expansion

Pressure Effect. Figure 9 shows the relationship between the bed expansion and the superficial liquid velocity at four different pressures for glass beads of diameter 2.1 mm under $T = 23.5$ and 60°C. It can be seen that for a given temperature and particle size, the bed expansion increases with an increase in the liquid velocity and pressure. Based on Eq. 7, F_{DS} increases with pressure and liquid velocity, while F_{eg} decreases with pressure, which leads to an increase in ϵ. In Figure 9, comparing the bed expansion at 0.1 and 20 MPa at the same liquid velocity, it is seen that the bed height at 0.1 MPa is about 20–30% lower than that at 20 MPa.

In Figure 10, it can be seen that at a given temperature the higher liquid velocities exhibit a greater effect of pressure on the bed expansion. This phenomenon can be attributed to effects on the Reynolds number, and thus on drag forces,

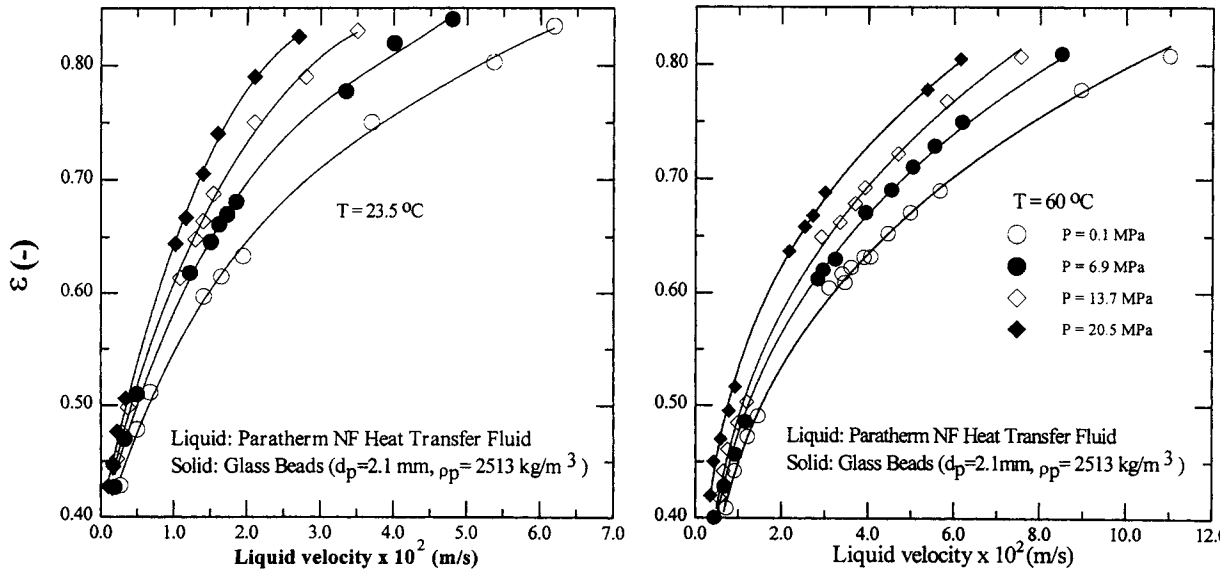

Figure 9. Pressure effects on the bed expansion for $d_p = 2.1$ mm at $T = 23.5$ and 60°C.

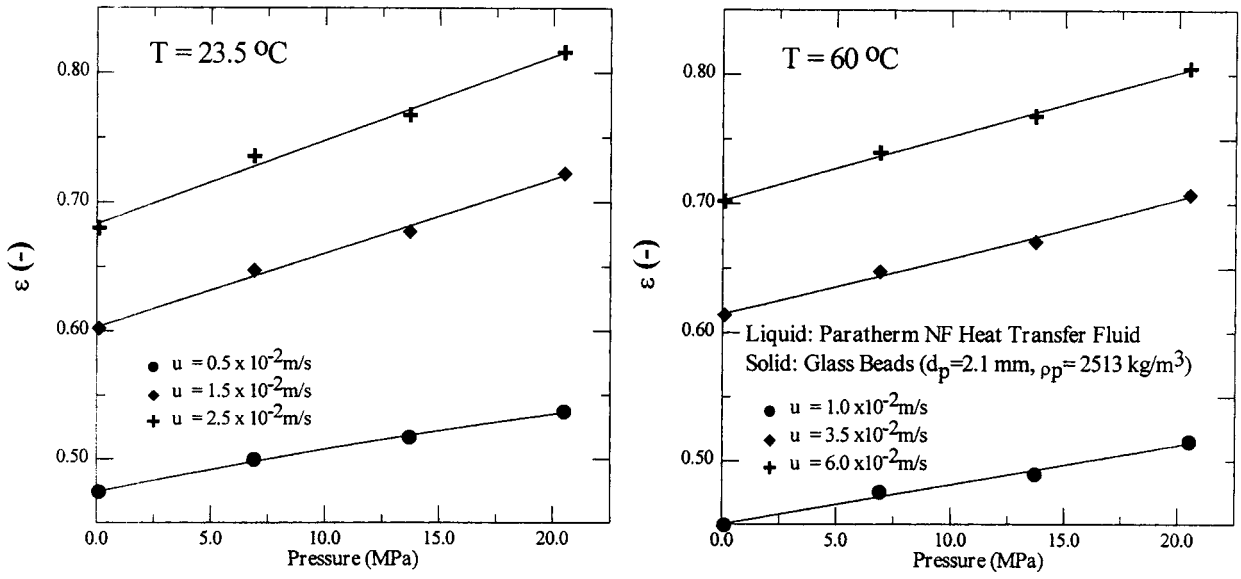

Figure 10. Pressure effects on the bed expansion for 2.1-mm glass beads at various liquid velocities and $T = 23.5$ and 60°C.

from variations in pressure and liquid velocity. To illustrate, the force balance equation (Eq. 7) is rearranged to

$$\epsilon^{4.7} = \frac{F_{DS}}{F_{eg}} = \frac{C_D\left(\frac{1}{2}\rho_f u^2\right)\left(\frac{1}{4}\pi d_p^2\right)}{F_{eg}}. \tag{12}$$

Consider liquid flows at velocities, u and xu (where $x > 1$), which fluidize a bed of particles at two different pressures but the same temperature. The change in bed voidage between low and high liquid velocities at a given pressure can be quantified by the following relationship:

$$\epsilon_1^{4.7} - \epsilon_2^{4.7} = \frac{F_{DS1} - F_{DS2}}{F_{eg}} = \frac{\Delta F}{F_{eg}}. \tag{13}$$

The property measurement of the liquid reflects that F_{eg} can be considered as constant due to insignificant effects of pressure and liquid velocity at a given temperature. F_{DS}, however, is a complex function of pressure and liquid velocity, as liquid velocity has both positive and negative effects on F_{DS} through the liquid properties and C_D, and pressure has positive effects on F_{DS} through C_D and ρ_f. Note that C_D within the range of bed expansion of this study is very sensitive to the Reynolds number ($0.1 < Re < 22$), as shown in Figure 11; hence, one only compares the change in drag force (ΔF). Based on the prescribed conditions, consider four drag coefficients shown in Figure 11: C_{D1}^l, C_{D1}^h, C_{D2}^l, and C_{D2}^h. Subscripts 1 and 2 represent the high and low liquid velocities, and the superscripts l and h represent the low and high pressures, respectively. The differences between drag coefficients at high and low pressures for two liquid velocities, ΔC_1 and ΔC_2, are defined below:

$$C_{D1}^h = C_{D1}^l + \Delta C_1 \tag{14}$$

$$C_{D2}^h = C_{D2}^l + \Delta C_2 \tag{15}$$

At low pressure, the change in drag force from low liquid velocity to high liquid velocity can be given by

$$\Delta F' = F_{DS1}^l - F_{DS2}^l = (x^2 C_{D1}^l - C_{D2}^l)\left(\frac{\pi \rho_f^l d_p^2 u^2}{8}\right). \tag{16}$$

At high pressure, by substituting Eqs. 14 and 15, the change in drag force from low liquid velocity to high liquid velocity can be obtained from

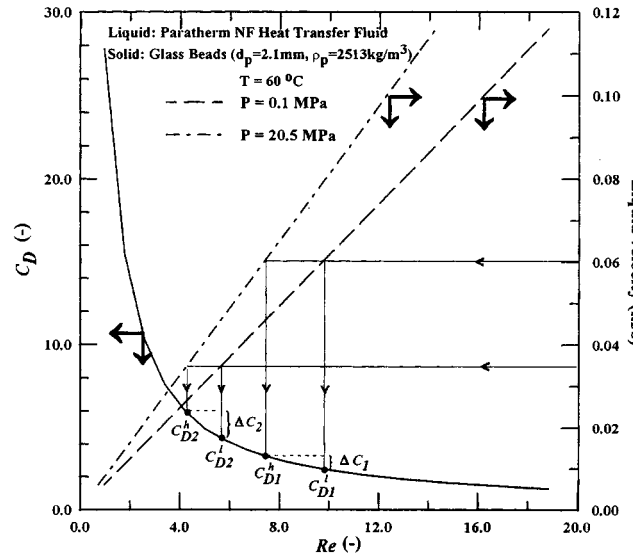

Figure 11. Variations of the drag coefficient and Reynolds number with the liquid velocity for $d_p = 2.1$ mm at $T = 60$°C and $P = 0.1$ and 20.5 MPa.

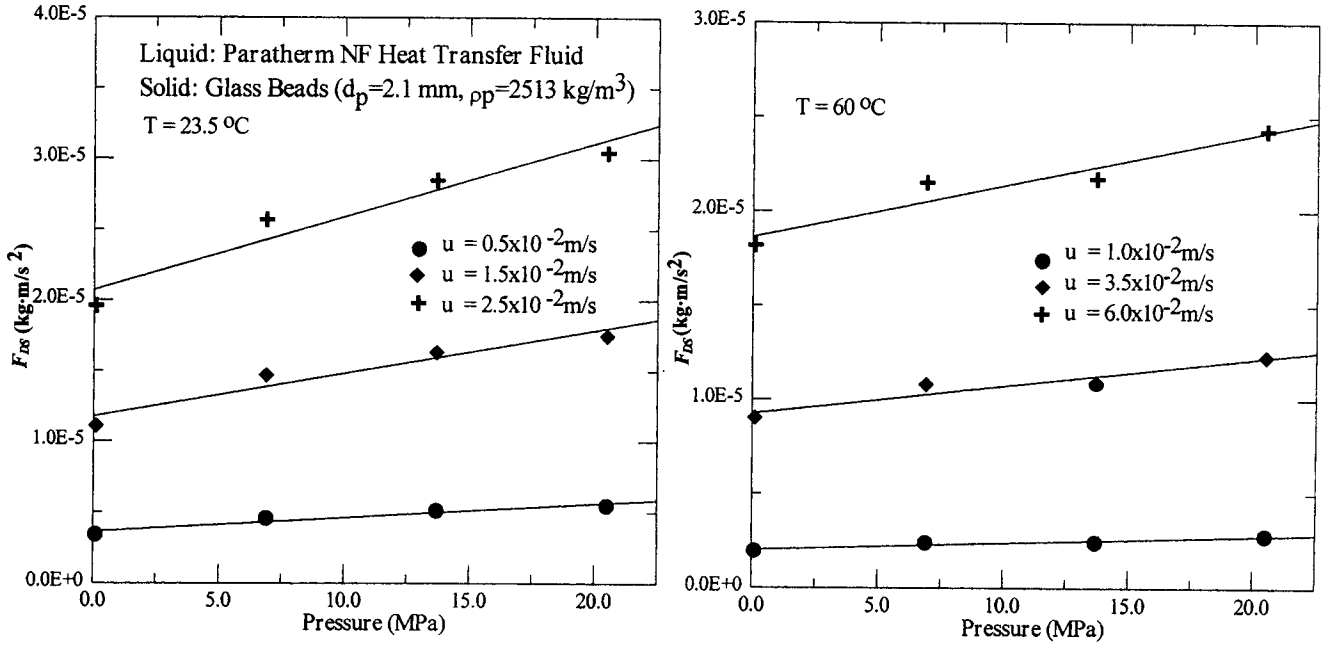

Figure 12. Pressure effects on F_{DS} under various liquid velocities at $T = 23.5$ and 60°C.

$$\Delta F^h = F^h_{DS1} - F^h_{DS2} = (x^2 C^h_{D1} - C^h_{D2})\left(\frac{\pi \rho_f^h d_p^2 u^2}{8}\right)$$

$$= (x^2 C^l_{D1} + x^2 \Delta C_1 - C^l_{D2} - \Delta C_2)\left(\frac{\pi \rho_f^h d_p^2 u^2}{8}\right)$$

$$\approx \Delta F^l + (x^2 \Delta C_1 - \Delta C_2)\left(\frac{\pi \rho_f^h d_p^2 u^2}{8}\right). \quad (17)$$

It can be seen from Figure 12 that the increase in F_{DS} with increasing pressure at a higher liquid velocity is greater than that at a lower liquid velocity. This behavior means that ΔF^h is always larger than ΔF^l, and $x^2 \Delta C_1 - \Delta C_2$ must be positive. In fact, data presented in Figure 11 support the preceding observation, and the value of $x^2 \Delta C_1 - \Delta C_2$ is always found to be positive.

Another direct approach to compare ΔF^h and ΔF^l is to construct a figure relating *Re*, drag force, and liquid velocity, as shown in Figure 13. From this figure, one can choose any two liquid velocities and draw two horizontal lines that intersect the pressure lines to obtain the corresponding Reynolds numbers. From the Reynolds numbers, the drag forces can be evaluated and the ΔF^h and ΔF^l can be determined. From this figure, one always obtained a larger value for ΔF^h, which implies that a higher liquid velocity yields a larger effect on pressure. It also explains that at higher Reynolds numbers, the effects of pressure on bed expansion are lesser. A more detailed analysis of the pressure effects on bed expansion is given in Appendix A.

Figures 14 and 15 show that at a given temperature and liquid velocity, the larger particle size exhibits a larger effect of pressure on the bed expansion. Equation 7 can also be applied to illustrate this phenomenon. Assume that particles of two different sizes are used as solids in a fluidized bed operated at two different pressures, but at the same temperature and velocity. The change in bed voidage between these two particle sizes at low and high pressure is then given by

$$(\epsilon_S^l)^{4.7} - (\epsilon_B^l)^{4.7} = \left[\frac{F^l_{DS}}{F_{eg}}\right]_S - \left[\frac{F^l_{DS}}{F_{eg}}\right]_B$$

$$= \left[\frac{3\rho_f u^2}{4(\rho_p - \rho_f)}\right]\left(\frac{C^l_{DS}}{d_S} - \frac{C^l_{DB}}{d_B}\right) \quad (18)$$

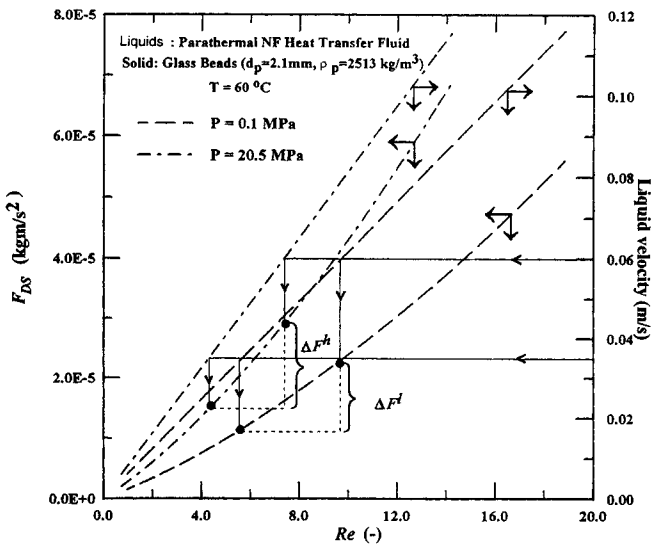

Figure 13. Variations of the drag force and Reynolds number with the liquid velocity for $d_p = 2.1$ mm at $T = 60$°C and $P = 0.1$ and 20.5 MPa.

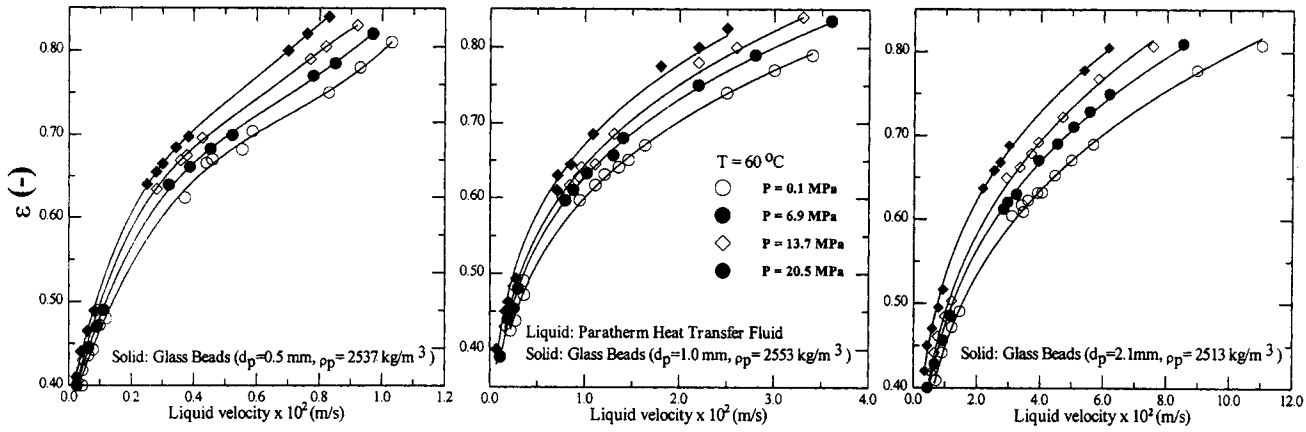

Figure 14. Pressure effects on the bed expansion for different particle sizes (d_p = 0.5, 1.0 and 2.1 mm) at T = 60°C.

$$(\epsilon_S^h)^{4.7} - (\epsilon_B^h)^{4.7} = \left[\frac{F_{DS}^h}{F_{eg}}\right]_S - \left[\frac{F_{DS}^h}{F_{eg}}\right]_B = \left[\frac{3\rho_f u^2}{4(\rho_p - \rho_f)}\right]\left(\frac{C_{DS}^h}{d_S} - \frac{C_{DB}^h}{d_B}\right), \quad (19)$$

where subscripts B and S represent, respectively, the large and small particles. The differences in drag coefficients between high pressure and low pressure for two particle sizes are denoted as ΔC_S and ΔC_D, as shown in Figure 16 and expressed below:

$$C_{DS}^h = C_{DS}^l + \Delta C_S \quad (20)$$

$$C_{DB}^h = C_{DB}^l + \Delta C_B. \quad (21)$$

Substituting Eqs. 20 and 21 into Eq. 19, yields

$$(\epsilon_S^h)^{4.7} - (\epsilon_B^h)^{4.7} = \left[\frac{3\rho_f u^2}{4(\rho_p - \rho_f)}\right]\left[\left(\frac{C_{DS}^l}{d_S} - \frac{C_{DB}^l}{d_D}\right) + \left(\frac{\Delta C_S}{d_S} - \frac{\Delta C_B}{d_B}\right)\right]$$

$$\approx (\epsilon_S^l)^{4.7} - (\epsilon_B^l)^{4.7} + \left(\frac{3\rho_f u^2}{4(\rho_p - \rho_f)}\right)\left(\frac{\Delta C_S}{d_S} - \frac{\Delta C_B}{d_B}\right). \quad (22)$$

From Figure 16, it can be seen that ΔC_S is always larger than ΔC_B. Since d_S is smaller than d_B, the value of $\Delta C_S/d_S - \Delta C_B/d_B$ is positive; therefore, the effect of pressure on bed expansion for small particles is more significant than that for large particles at a given velocity and temperature. It also means that a larger Reynolds number gives rise to a lesser

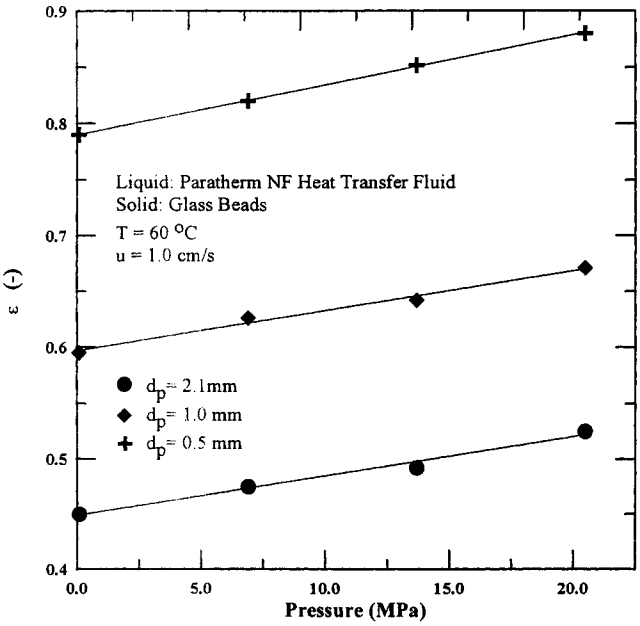

Figure 15. Pressure effects on the bed expansion for different particle sizes (d_p = 0.5, 1.0 and 2.1 mm) at T = 60°C.

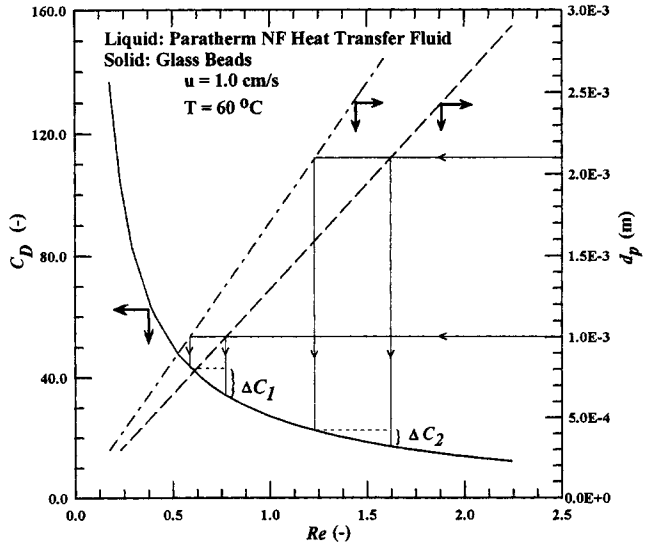

Figure 16. Variations of the drag coefficient and Reynolds number with the particle size for u = 1.0 m/s at T = 60°C and P = 0.1 and 20.5 MPa.

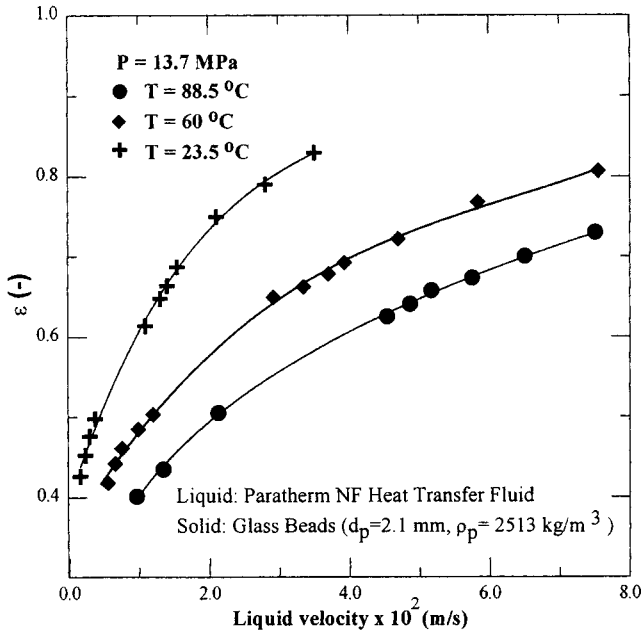

Figure 17. Temperature effects on the bed expansion under P = 13.7 MPa for 2.1-mm glass beads.

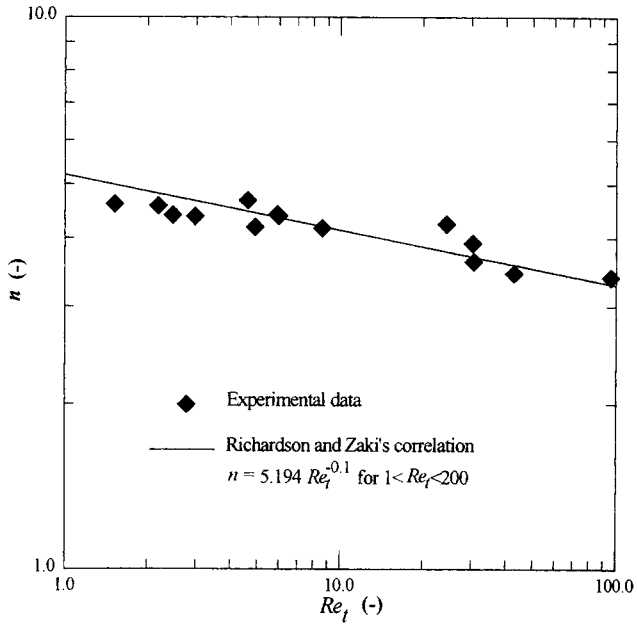

Figure 18. Experimental results vs. prediction by the Richardson and Zaki correlation.

effect of pressure on the increasing rate of bed expansion. A detailed analysis of pressure effects on bed expansion of different particles is presented in Appendix B.

Temperature Effect. Figure 17 shows the temperature effect on the bed expansion at the pressure of 13.7 MPa using 2.1-mm glass beads. The figure shows that for a given liquid velocity the bed expansion at low temperatures is more prominent than that at high temperatures. An increase in temperature reduces the liquid density and viscosity, which causes F_{eg} and F_{DS} to decrease; however, as the temperature increases, the rate of change for density is less than that for viscosity, yielding an increase in the ratio of F_{eg} to F_{DS}. The bed expansion is therefore greater at a lower temperature. Comparing the bed expansion at 23.5 and 88.5°C at the same liquid velocity, it can be seen that the bed expansion at 23.5°C is about 50% higher than that at 88.5°C. This implies that the temperature effect on bed expansion is more significant than the pressure effect at a given liquid velocity, which can also be seen in Figure 9.

Comparison. The Richardson and Zaki (1954) equation given below is applied to examine the bed expansion:

$$\frac{u}{u_t} = \epsilon^n, \tag{23}$$

where n is a function of the Reynolds number based on the terminal velocity of the particle, Re_t, and the ratio of d_p/D. Considering the wall effect and the ratio of particle to column size, the comparison of experimental results of bed expansion with the Richardson and Zaki correlation is presented in Figure 18. The figure shows that, using the liquid properties evaluated at the operating conditions, the bed expansion can be well predicted by Eq. 23.

Concluding Remarks

The fundamental characteristics of liquid–solid fluidization at high pressures (up to 21 MPa) and moderate temperatures (up to 89°C) are investigated. Properties under study include u_{mf}, bed voidage at minimum fluidization, and bed expansion. Devices for *in situ* measurements of the physical properties of liquid in the column are developed and measurements are carried out to quantify the pressure and temperature effects on the fluidization behavior. The results indicate that under high pressures and moderate temperatures, liquid–solid fluidization is significantly affected by the variation of the liquid density and viscosity. As the pressure increases, the liquid viscosity and density increase, yielding an increased drag force and buoyancy force on the particles, and hence a decreasing u_{mf} and an increasing bed expansion for a given liquid flow rate. An increase in temperature has the opposite effect on the liquid physical properties, which results in an increase in u_{mf} and a decrease in the bed expansion for a given liquid flow rate. Based on the measured liquid physical properties under bed operating conditions, the study indicates that the liquid velocity and bed voidage at minimum fluidization and the bed expansion can be well predicted, respectively, by the correlations of Chitester et al. (1984) and Richardson and Zaki (1954).

Acknowledgment

The work was supported by National Science Foundation grants CTS-9200793 and CTS-9528380. We are grateful to Dr. P.-J. Jiang and Mr. X. Luo for helpful assistance on the experimental work, and Professor R. F. Mudde for constructive discussion.

Notation

Ar = Archimedes number $d_p^3 \rho_l (\rho_p - \rho_f) g/\mu^2$
D = diameter of column, mm
d_p = diameter of particle, mm

g = gravitational acceleration, m/s^2
l = length of aluminum tube defined in Figure 2, m
l_1 = length of aluminum tube defined in Figure 2, m
l_2 = length of aluminum tube defined in Figure 2, m
p = pressure (MPa)
Re_{mf} = Reynolds number based on minimum fluidization velocity $\rho_f u_{mf} d_p/\mu$
T_b = boiling point, °C
u_t = particle terminal velocity, m/s
x = ratio of high liquid velocity to low liquid velocity

Greek letters

γ = numerical exponent
ϵ = bed voidage
μ = liquid viscosity, kg/m·s
ρ_p = particle density, kg/m^3
σ = surface tension, N/m

Literature Cited

Chitester, D. C., R. M. Kornosky, L.-S. Fan, and J. P. Danko, "Characteristics of Fluidization at High Pressure," *Chem. Eng. Sci.*, **39**, 253 (1984).

Clift, R., J. R. Grace, and M. E. Weber, *Bubble Drops and Particles*, Academic Press, New York (1978).

Di Felice, R., "Hydrodynamics of Liquid Fluidization," *Chem. Eng. Sci.*, **50**, 1213 (1995).

Ewell, R. H., and H. Eyring, "Theory of the Viscosity of Liquids as a Function of Temperature and Pressure," *J. Chem. Phys.*, **5**, 726 (1937).

Fan, L.-S., *Gas-Liquid-Solid Fluidization Engineering*, Butterworths, Stoneham, MA (1989).

Foscolo, P. U., L. G. Gibilaro, and S. P. Waldram, "A Unified Model for Particulate Expansion of Fluidized Beds and Flow in Fixed Porous Media," *Chem. Eng. Sci.*, **38**, 1251 (1983).

Grace, J. R., "Fluidized-Bed Hydrodynamics," *Handbook of Multiphase Systems*, G. Hestroni, ed., Hemisphere, Washington, DC (1982).

Institute of Gas Technology, Coal Conversions Systems, *Technical Data Book*, Chicago Sec. IVB, Chicago, IL (1978).

Khan, A. R., and J. F. Richardson, "The Resistance to Motion of a Solid Sphere in a Fluid," *Chem. Eng. Commun.*, **62**, 135 (1987).

Kwauk, M., *Fluidization-Idealised and Bubbleless with Application*, Ellis Horwood, Chichester, England (1992).

Oseen, C. W., "Über die Stokes'sche Formel und über eine verwandte Aufgabe in der Hydrodynamik," *Ark. Mat. Astron. Fys.*, **6**, 29 (1910).

Richardson, J. F., and M. A. Jeronimo, "Velocity-Voidage Relations for Sedimentation and Fluidization," *Chem. Eng. Sci.*, **34**, 1419 (1979).

Richardson, J. F., "Incipient Fluidization and Particulate Systems," *Fluidization*, J. F. Davidson and D. Harrison, eds., Academic Press, New York, p. 26 (1971).

Richardson, J. F., and W. Z. Zaki, "Sedimentation and Fluidization: I," *Trans. Instn. Chem. Engrs.*, **32**, 35 (1954).

Rietema, K., "Science and Technology of Dispersed Two-Phase Systems: I and II," *Chem. Eng. Sci.*, **37**, 1125 (1982).

Stokes, G. G., "On the Effect of Internal Friction of Fluids on the Motion of Pendulums," *Trans. Cambridge Phil. Soc.*, **9**, 8 (1851).

Wen, C. H., and Y. H. Yu, "Mechanics of Fluidization," *Chem. Eng. Prog. Symp. Ser.*, **62**, 100 (1966).

Appendix A

These Appendices provide the proof that at a given temperature, the effect of pressure on the bed expansion increases as the liquid velocity increases. This Appendix considers the case of constant particle diameter with varying liquid velocity. Appendix B considers the case of constant liquid velocity with varying particle diameter.

In liquid–solid fluidization, the bed expansion can be described by

$$\epsilon^n = \frac{F_{DS}}{F_{eg}} = \frac{C_D\left(\frac{\pi}{4}d^2\right)\left(\frac{1}{2}\rho_f u^2\right)}{\frac{\pi}{6}g(\rho_p - \rho_f)d^3}, \tag{A1}$$

where $n > 1$. The term $\rho_p - \rho_f$ is approximated as a constant. Equation A1 can be expressed as

$$\epsilon^n \propto C_D \rho_f u^2. \tag{A2}$$

For Stokes' regime

The drag coefficient for a single particle in an infinite fluid is given by

$$C_D = \frac{24}{Re} = \frac{24\mu}{\rho_f u d}. \tag{A3}$$

Based on the present measurements, the liquid viscosity can be related to pressure by

$$\mu = \mu_{1_{(P=1\,\mathrm{atm})}} * P^m \propto P^m, \tag{A4}$$

where $m > 0$ and $P > 1$. Substituting Eqs. A4 and A3 into Eq. A2 yields

$$\epsilon^n \propto \frac{24\mu\rho_f u^2}{\rho_f u d} \propto \mu u \propto P^m u. \tag{A5}$$

Therefore,

$$\epsilon \propto P^{m/n} u^{1/n}. \tag{A6}$$

Consider two fluidizing velocities, u_1 and u_2, that differ by Δu, that is,

$$u_1 = u_2 + \Delta u. \tag{A7}$$

The Taylor expansion of $\epsilon(u, P)$ around $u = u_2$ gives

$$\epsilon(u_1, P) = \epsilon(u_2, P) + \left.\frac{\partial \epsilon}{\partial u}\right|_{u_2} \Delta u + \cdots. \tag{A8}$$

For high pressures (indicated by subscript h), the increase in voidage $\Delta\epsilon_h$ from u_2 and u_1 is given by

$$\Delta\epsilon_h = \epsilon(u_1, P_h) - \epsilon(u_2, P_h) = \left.\frac{\partial \epsilon}{\partial u}\right|_{u_2} \Delta u. \tag{A9}$$

Hence,

$$\Delta\epsilon_h \propto \left(\frac{1}{n} u_2^{(1/n)-1}\right) P_h^{m/n} \Delta u. \tag{A10}$$

For low pressures (indicated by subscript l), the increase in voidage $\Delta\epsilon_l$ from u_2 to u_1 is given by

$$\Delta\epsilon_l \propto \left(\frac{1}{n}u_2^{(1/n)-1}\right)P_l^{m/n}\Delta u. \tag{A11}$$

Subtracting $\Delta\epsilon_l$ in Eq. A11 from $\Delta\epsilon_h$ in Eq. A10 gives

$$\Delta\epsilon_h - \Delta\epsilon_l \propto \left(\frac{\Delta u}{n}\right)(u_2^{(1/n-1)})(P_h^{m/n} - P_l^{m/n}). \tag{A12}$$

Since $n > 1$ and $m > 0$, Eq. A12 leads to

$$P_h^{m/n} - P_l^{m/n} > 0, \tag{A13}$$

which proves that

$$\Delta\epsilon_h > \Delta\epsilon_l. \tag{A14}$$

That is a larger increase in bed voidage at high pressures than at low pressures.

For 1 < Re < 500 regime

The drag coefficient can be approximated by

$$C_D = \frac{24}{Re}(1 + aRe^b), \tag{A15}$$

where $0 < a$ and $b < 1$.

Substituting Eqs. A4 and A15 into Eq. A2 gives

$$\epsilon \propto (P^{m/n}u^{1/n})(1 + aRe^b)^{1/n}$$
$$\propto (P^{m/n}u^{1/n})(1 + \alpha u^b - P^{-bm})^{1/n}, \tag{A16}$$

where $\alpha = a(\rho_f d)^b$ is virtually a constant, since the pressure effect on density is much less than that on viscosity. With the Taylor expansion of $\epsilon(u, P)$ and rearrangement, the increase in voidages $\Delta\epsilon_h$ and $\Delta\epsilon_l$ from u_2 to u_1, can be expressed by

$$\Delta\epsilon_h \propto \left(\frac{1}{n}u_2^{(1/n)-1}\right)(P_h^m + K_h)^{1/n}\left(1 + \frac{bK_h}{P_h^m + K_h}\right)\Delta\mu, \tag{A17}$$

where $K_h = \alpha u_2^b P_h^{(1-b)m}$ and $K_l = \alpha u_2^b P_l^{(1-b)m}$. Since $b < 1$, K increases monotonically with pressure. The factor $(P^m + K)^{1/n}\,[1 + bK/(P^m + K)]$ would increase monotonically with pressure. Thus, the bed expansion is greater at higher pressures, that is, $\Delta\epsilon_h > \Delta\epsilon_l$.

For Re > 500 regime

The drag coefficient can be approximated by

$$C_D \simeq 0.4. \tag{A19}$$

Substituting Eq. A19 into Eq. A2 leads to

$$\epsilon^n \propto \rho_f u^2. \tag{A20}$$

Based on the measurements, the liquid density can be related to pressure by

$$\rho_f = \rho_{f_{(P=1\,\mathrm{atm})}} * P^\gamma \propto P^\gamma, \tag{A21}$$

where $\gamma > 0$.

Substituting Eq. 21 into Eq. A20 yields

$$\epsilon \propto P^{\gamma/n}u^{2/n}. \tag{A22}$$

With the Taylor expansion of $\epsilon(u, P)$, and following the same procedures as earlier, the difference between $\Delta\epsilon_h$ and $\Delta\epsilon_l$ can be expressed by

$$\Delta\epsilon_h - \Delta\epsilon_l \propto \left(\frac{\Delta u}{n}\right)(u_w^{(2/n)-1})(P_h^{\gamma/n} - P_l^{\gamma/n}). \tag{A23}$$

Since $\gamma > 0$ and $n > 1$, it proves that

$$\Delta\epsilon_h > \Delta\epsilon_l. \tag{A24}$$

Appendix B

Consider that the liquid velocity is constant and that the term $\rho_p - \rho_f$ can be approximated as constant for all pressures. Equation A1 can be simplified to

$$\epsilon^n \propto \frac{C_D\rho_f}{d}. \tag{B1}$$

For Stokes' regime

Substituting Eqs. A3 and A4 into Eq. B1 yields

$$\epsilon \propto P^{m/n}d^{-(2/n)}. \tag{B2}$$

Consider two particle sizes, d_1 and d_2, that differ by Δd, that is,

$$d_1 = d_2 + \Delta d. \tag{B3}$$

With the Taylor expansion of $\epsilon(d, P)$, and following the same procedures as given in Appendix A, the difference between $\Delta\epsilon_h$ and $\Delta\epsilon_l$ can be expressed by

$$\Delta\epsilon_h - \Delta\epsilon_l \propto \left(\frac{2}{n}d_2^{-(2/n)-1}\right)(P_h^{m/n} - P_l^{m/n})\Delta d. \tag{B4}$$

Since $m > 0$ and $n > 1$, it proves that

$$\Delta\epsilon_h > \Delta\epsilon_l. \tag{B5}$$

For 1 < Re < 500 regime

Substituting Eqs. A4 and A15 into Eq. B1 gives

$$\epsilon \propto (P^{m/n}d^{-(2/n)})(1 + aRe^b)^{1/n}$$
$$\propto (P^{m/n}d^{-(2/n)})(1 + \lambda d^b P^{-bm})^{1/n} \tag{B6}$$

where $\lambda = a(\rho_f u)^b$ is a constant. With the Taylor expansion of $\epsilon(d, P)$ and rearrangement, the increase in voidages $\Delta\epsilon_h$ and $\Delta\epsilon_l$ from d_1 to d_2, is given by

$$\Delta\epsilon_h \propto \left(\frac{2}{n} d_2^{-(2/n)-1}\right)(P_h^m + H_h)^{1/n}\left(2 - \frac{bH_h}{P_h^m + H_h}\right)\Delta d \quad \text{(B7)}$$

$$\Delta\epsilon_l \propto \left(\frac{2}{n} d_2^{-(2/n)-1}\right)(P_l^m + H_l)^{1/n}\left(2 - \frac{bH_l}{P_l^m + H_l}\right)\Delta d, \quad \text{(B8)}$$

where $H_h = \lambda d_2^b P_h^{(1-b)m}$ and $H_l = \lambda d_2^b P_l^{(1-b)m}$. Since $b < 1$, H increases monotonically with pressure. Therefore, by comparing Eqs. B7 and B8, it proves that $\Delta\epsilon_h > \Delta\epsilon_l$.

For Re > 500 regime

Substituting Eqs. A19 and A21 into Eq. B1 yields

$$\epsilon \propto P^{\gamma/n} d^{-(1/n)}. \quad \text{(B9)}$$

With the Taylor expansion of $\epsilon(d, P)$ and following the same procedures as before, the difference between $\Delta\epsilon_h$ and $\Delta\epsilon_l$ can be expressed by

$$\Delta\epsilon_h - \Delta\epsilon_l \propto \left(\frac{\Delta d}{n}\right)(d_2^{-(1/n)-1})(P_h^{\gamma/n} - P_l^{\gamma/n}). \quad \text{(B10)}$$

Hence, with $\gamma > 0$ and $n > 1$, it proves that $\Delta\epsilon_h > \Delta\epsilon_l$.

Manuscript received Jan. 16, 1996, and revision received by July 12, 1996.